

ON THE INCORPORATION OF SPATIAL INFORMATION TO ENDMEMBER EXTRACTION: SURVEY AND ALGORITHM COMPARISON

Antonio Plaza, Gabriel Martín

Department of Computer Science,
University of Extremadura,
E-10071 Cáceres, Spain.

Maciel Zortea

Department of Mathematics and Statistics,
University of Tromsø,
N-9037, Tromsø, Norway.

ABSTRACT

Several well-known algorithms have been used for endmember extraction and spectral unmixing of hyperspectral imagery by considering only the spectral properties of the data when conducting the search. However, it might be beneficial to incorporate the spatial arrangement of the data in the development of endmember extraction and spectral unmixing algorithms. In this paper, we provide a survey on the use of spatial information in endmember extraction and further compare six different algorithms (three of which only use spectral information) in order to substantiate the impact of using spatial-spectral information versus only spectral information when searching for image endmembers. The comparison is carried out using a synthetic hyperspectral scene with spatial patterns generated using fractals, and a real hyperspectral scene collected by NASA's Airborne Visible Infra-Red Imaging Spectrometer (AVIRIS).

Index Terms— Spectral mixture analysis, hyperspectral imaging, endmember extraction, spatial-spectral analysis

1. INTRODUCTION

Spectral mixture analysis [1] is a popular approach to characterize mixed pixels in remotely sensed hyperspectral scenes. This approach first identifies a collection of spectrally pure constituent spectra, called *endmembers* in the literature [2], and then expresses the measured spectrum of each mixed pixel as a combination of endmembers weighted by fractions or *abundances* that indicate the proportion of each endmember present in the pixel. Over the last decade, several algorithms have been developed for automatic or semi-automatic extraction of spectral endmembers directly from the image data (image endmembers) [2, 3]. However, few available techniques consider the spatial information when searching for endmembers. In turn, one of the distinguishing properties of hyperspectral data is the spatial arrangement of the data. Subsequently, endmember extraction algorithms can benefit from an integrated framework in which both the spatial and the spectral information is considered.

To the best of our knowledge, only a few attempts exist in the literature aimed at including the spatial information in the process of extracting spectral endmembers. Extended morphological operations [4] have been used as a baseline to develop an automatic morphological endmember extraction (AMEE) algorithm [5] for spatial-spectral endmember extraction. Also, spatial averaging of spectrally similar endmember candidates found via singular value decomposition (SVD) was used in the development of the spatial spectral endmember extraction (SSEE) algorithm [6]. Recently, a spatial preprocessing (SPP) algorithm [7] has been proposed which estimates, for each pixel vector in the scene, a spatially-derived factor that is used to weight the importance of the spectral information associated to each pixel in terms of its spatial context. The SPP is intended as a preprocessing module that can be used in combination with an existing spectral-based endmember extraction algorithm.

Despite the existence of several efforts and strategies aimed at inter-comparing spectral-based endmember extraction algorithms [2, 3], a cross-validation of algorithms using both spatial and spectral information is not yet available. Such study is important in order to fully substantiate the advantages of using spatial-spectral versus only spectral information when searching for image endmembers. In this paper, we focus on this issue and provide an experimental inter-comparison of the accuracy of six different endmember extraction algorithms, three of which use spatial-spectral information (AMEE, SSEE, and SPP). The SPP is used in this work as a preprocessing module for three classic spectral-based algorithms: N-FINDR [8], orthogonal subspace projection (OSP) [9], and vertex component analysis (VCA) [10]. These algorithms are representative of a class of convex geometry-based techniques and are fully automated, allowing us to draw *fair* comparisons with regards to spatial-spectral algorithms. The algorithm comparison presented in this work is carried out in terms of endmember signature purity, using a synthetic hyperspectral scene with spatial patterns generated using fractals, and a real hyperspectral scene collected by NASA's Airborne Visible Infra-Red Imaging Spectrometer (AVIRIS) over the Cuprite mining district in Nevada.

2. ALGORITHMS

Three spectral-based algorithms (N-FINDR, OSP, VCA) and three spatial-spectral endmember extraction algorithms (AMEE, SSEE, SPP) will be used in our comparison. The number of endmembers to be extracted, p , is an input parameter for all algorithms, while the AMEE, SSE and SPP have additional input parameters related with the definition of spatial context around each pixel in the scene.

2.1. N-FINDR

The N-FINDR [8] algorithm looks for the set of pixels with the largest possible volume by *inflating* a simplex inside the data. The procedure begins with a random initial selection of p pixels. Every pixel in the image must be evaluated in order to refine the estimate of endmembers, looking for the set of pixels that maximizes the volume of the simplex defined by selected endmembers. The volume of simplex is calculated with every pixel in place of each endmember. The corresponding volume is calculated for every pixel in each endmember position by replacing that endmember and finding the resulting volume. If the replacement results in an increase of volume, the pixel replaces the endmember. This procedure is repeated until there are no more endmember replacements.

2.2. OSP

The OSP [9] algorithm starts by selecting the pixel vector with maximum length in the scene as the first endmember. Then, it looks for the pixel vector with the maximum absolute projection in the space orthogonal to the space linearly spanned by the initial pixel, and labels that pixel as the second endmember. A third endmember is found by applying an orthogonal subspace projector to the original image, where the signature that has the maximum orthogonal projection in the space orthogonal to the space linearly spanned by the first two endmembers. This procedure is repeated until the desired number of endmembers, p , is found.

2.3. VCA

The VCA [10] also makes use of the concept of orthogonal subspace projections. However, as opposed to the OSP algorithm, the VCA exploits the fact that the endmembers are the vertices of a simplex, and that the affine transformation of a simplex is also a simplex [10]. As a result, VCA models the data using a positive cone, whose projection onto a properly chosen hyperplane is another simplex whose vertices are the final endmembers. After projecting the data onto the selected hyperplane, the VCA projects all image pixels to a random direction and uses the pixel with the largest projection as the first endmember. The other endmembers are identified in sequence by iteratively projecting the data onto a direction orthogonal to the subspace spanned by the endmembers

already determined. Each new endmember is then selected as the pixel corresponding to the extreme projection, and the procedure is repeated until p endmembers are found.

2.4. AMEE

The AMEE [5] algorithm runs on the full hyperspectral data cube with no dimensional reduction, and begins by searching spatial neighborhoods (according to a square window neighborhood with size given as an input parameter) around each pixel in the image for the most spectrally pure and mostly highly mixed pixel. This task is performed by using extended mathematical morphology operators [4] of dilation and erosion, respectively. Each spectrally pure pixel is assigned an “eccentricity” value, which is calculated as the spectral angle distance between the most spectrally pure and mostly highly mixed pixel for the given spatial neighborhood. This process is repeated iteratively for larger spatial neighborhoods up to a maximum size that is pre-determined. At each iteration the “eccentricity” values of the selected pixels are updated. The final endmember set is obtained by applying a threshold to the resulting greyscale “eccentricity” image. The final p endmembers are extracted after a region growing process.

2.5. SSEE

The SSEE [6] algorithm comprises four steps. First, it applies singular value decomposition (SVD) to determine a set of eigenvectors that describe most of the spectral variance of image subsets. Then, it projects the entire image data onto the compiled eigenvector set to determine a set of candidate endmember pixels. In a third step, the algorithm analyzes the spatial and spectral characteristics of the candidate endmember set to average spectrally similar endmember candidates that are spatially related, according to a window neighborhood with size given as an input parameter. Finally, the endmember set derived in the previous step is reordered based on spectral angle, thus listing endmember candidates in order of spectral similarity (from highest to lowest similarity). In our implementation, we have used the OSP algorithm as a criterion to select the final set of p endmembers.

2.6. SPP

The SPP [7] serves as a preprocessing module which can be combined with existing spectral-based algorithms such as the N-FINDR, OSP and VCA. The method estimates, for each input pixel vector, a scalar factor which is intimately related to the spatial similarity between the pixel and its spatial neighbors, and then uses this scalar factor to spatially weight the spectral information associated to the pixel (thus modifying the original simplex). In this method, the spatial coordinates of the endmembers extracted from the spatially preprocessed image are retained, but the spectral signatures associated to

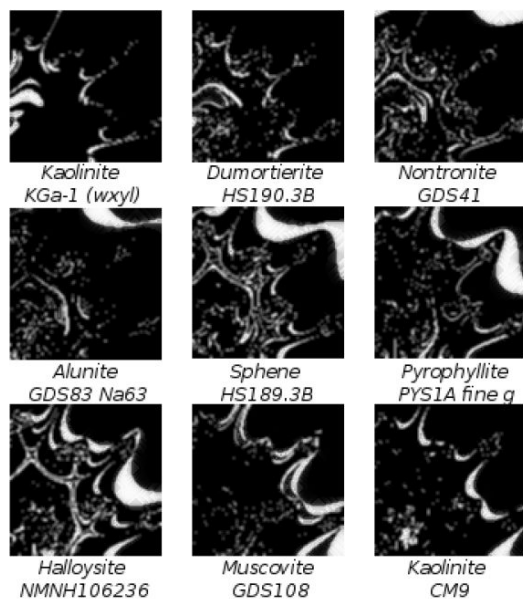


Fig. 1. Fractional abundance distributions used in the generation of a synthetic scene used in experiments.

those spatial coordinates (endmembers) are obtained from the original hyperspectral scene.

3. EXPERIMENTAL RESULTS

3.1. Hyperspectral data sets

A synthetic hyperspectral scene has been created using fractals to generate distinct spatial patterns, which are then used to simulate linear mixtures of reflectance signatures selected from a spectral library compiled by the U.S. Geological Survey (USGS)¹. Fig. 1 shows the nine fractional abundances used in the generation of the scene, where black color indicates 0% abundance of the corresponding mineral, white color indicates 100% abundance of the mineral, and fractional abundances in each pixel of the scene sum to unity. Of all the mixed pixels (100×100) simulated in the synthetic scene, 41.54% are binary in nature (i.e. made up of two endmembers), 20.14% are made up of three endmembers, 18.21% are made up of four endmembers, and 20.08% are made up of five or more endmembers. Zero-mean Gaussian noise was added to the scenes in different signal to noise ratios (SNRs) –from 30:1 to 110:1– to simulate contributions from ambient (clutter) and instrumental sources, following the procedure described in [9].

The real hyperspectral scene used in experiments is the well-known AVIRIS Cuprite data set, available online in reflectance units². This scene has been widely used to validate

¹<http://speclab.cr.usgs.gov/spectral-lib.htm>

²<http://aviris.jpl.nasa.gov/html/aviris.freedata.html>

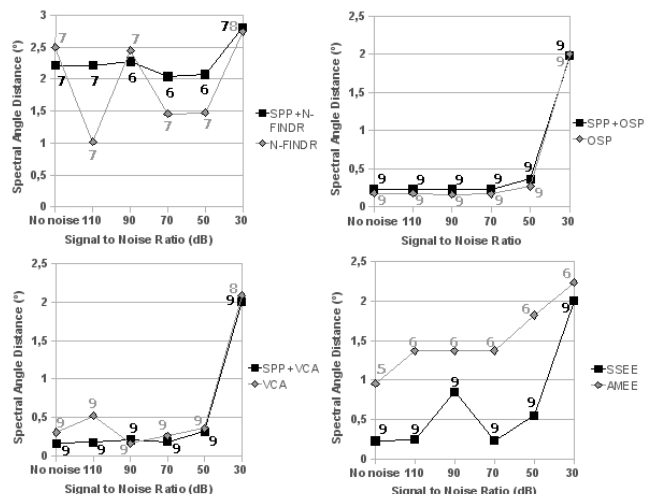


Fig. 2. Comparison of different endmember extraction algorithms in terms of signature purity, using the synthetic scene in Fig. 1 with different SNR values.

the performance of endmember extraction algorithms in the past [2, 3, 5, 6, 7, 8, 10]. The portion used in experiments comprises 350×350 pixels and a total of 188 reflectance channels (between 0.4 and $2.5 \mu\text{m}$) after removal of water absorption and noisy spectral bands.

3.2. Algorithm comparison

In order to ensure the fairest possible comparison, the best performance must be obtained from each alternative method. In this work, we have individually optimized each method to achieve the best possible results (by analyzing different spectral matching criteria) by testing all possible parameter values (within reasonable range values) and report the best result obtained for each algorithm with the considered scene. For illustrative purposes, Fig. 2 displays the spectral angle distance (SAD) between the endmembers extracted by different methods and reference USGS spectral signatures for the simulated scene in Fig. 1 without noise, and with simulated noise at different signal to noise ratios (SNRs). In the figure, lower SAD indicates higher spectral similarity. The number above each data point in Fig. 2 indicates how many extracted endmembers (out of $p = 9$) were actually matched to the reference USGS spectral signatures using the spectral similarity matching algorithm (SSMA) described in [2].

As shown by Fig. 2, the best overall results were obtained by the OSP algorithm (lower SAD scores and higher number of matched endmembers) followed very closely by SPP+OSP (spatial preprocessing followed by OSP), SPP+VCA, and SSEE. The AMEE provided better results than N-FINDR and SPP+N-FINDR. In this example, spatial preprocessing clearly improved the results provided by VCA, but did not significantly improve the results provided by OSP (which

Table 1. SAD-based spectral similarity scores (in degrees) between the USGS mineral spectra and their corresponding endmember pixels produced by several endmember extraction algorithms.

Algorithm	Alunite	Buddingtonite	Calcite	Kaolinite	Muscovite	Mean
N-FINDR	9.96°	7.71°	12.08°	13.27°	5.24°	9.65°
OSP	4.81°	4.16°	9.62°	11.14°	5.41°	7.03°
VCA	10.73°	9.04°	6.36°	14.05°	5.41°	9.12°
AMEE	4.81°	4.21°	9.54°	8.74°	4.61°	6.38°
SSEE	4.81°	4.16°	8.48°	11.14°	4.62°	6.64°
SPP+N-FINDR	12.81°	8.33°	9.83°	10.43°	5.28°	9.34°
SPP+OSP	4.95°	4.16°	9.96°	10.90°	4.62°	6.92°
SPP+VCA	12.42°	4.04°	9.37°	7.87°	6.18°	7.98°

were comparable to those obtained without using spatial preprocessing) and only improved the results provided by N-FINDR for the case in which no noise was simulated in the synthetic scene.

Table 1 tabulates the SAD scores (in degrees) obtained after comparing the USGS library spectra of five highly representative minerals in the Cuprite mining district (*alunite*, *buddingtonite*, *calcite*, *kaolinite* and *muscovite*) with the corresponding endmembers extracted by different algorithms from the AVIRIS Cuprite scene. The smaller the SAD values across the five minerals in Table 1, the better the results. It should be noted that Table 1 only displays the smallest SAD scores of all endmembers with respect to each USGS signature for each algorithm. For reference, the mean SAD values across all five USGS signatures is also reported. In all cases, the number of endmembers to be extracted was set to $p = 14$ after using the virtual dimensionality (VD) concept in [11]. Table 1 reveals that the AMEE provides very good results (all SAD scores below 10°), with the SSEE and the SPP+OSP being the algorithms that can provide comparable -but slightly worst- results. Table 1 also reveals that, in this real example, spatial preprocessing always improves the signature purity of the endmembers extracted by spectral-based algorithms. These results suggest the advantages of incorporating spatial information into the automatic extraction of image endmembers.

4. CONCLUSIONS AND FUTURE RESEARCH

In this paper, we have substantiated the impact of using spatial-spectral information versus only spectral information when searching for image endmembers. The results produced by the algorithms tested in this study have been analyzed and discussed in terms of endmember signature purity, using a synthetic hyperspectral scene with spatial patterns generated using fractals and a real hyperspectral scene collected by NASA's AVIRIS instrument over the Cuprite mining district in Nevada. Our experimental results indicate that spatial information can assist the selection of spectral endmembers by taking advantage of the existing spatial autocorrelation between image features. Further experiments with additional scenes should be conducted in order to validate the above remarks under different analysis scenarios.

5. REFERENCES

- [1] J. B. Adams, M. O. Smith, and P. E. Johnson, "Spectral mixture modeling: a new analysis of rock and soil types at the Viking Lander 1 site," *Journal of Geophysical Research*, vol. 91, pp. 8098–8112, 1986.
- [2] A. Plaza, P. Martinez, R. Perez, and J. Plaza, "A quantitative and comparative analysis of endmember extraction algorithms from hyperspectral data," *IEEE Transactions on Geoscience and Remote Sensing*, vol. 42, no. 3, pp. 650–663, 2004.
- [3] Q. Du, N. Raksuntorn, N.H. Younan, and R.L. King, "Endmember extraction for hyperspectral image analysis," *Applied Optics*, vol. 47, no. 28, pp. 77–84, 2008.
- [4] A. Plaza, P. Martinez, J. Plaza, and R. Perez, "Dimensionality reduction and classification of hyperspectral image data using sequences of extended morphological transformations," *IEEE Transactions on Geoscience and Remote Sensing*, vol. 43, no. 3, pp. 466–479, 2005.
- [5] A. Plaza, P. Martinez, R. Perez, and J. Plaza, "Spatial/spectral endmember extraction by multidimensional morphological operations," *IEEE Transactions on Geoscience and Remote Sensing*, vol. 40, no. 9, pp. 2025–2041, 2002.
- [6] D. M. Rogge, B. Rivard, J. Zhang, A. Sanchez, J. Harris, and J. Feng, "Integration of spatial-spectral information for the improved extraction of endmembers," *Remote Sensing of Environment*, vol. 110, no. 3, pp. 287–303, 2007.
- [7] M. Zortea and A. Plaza, "Spatial preprocessing for endmember extraction," *IEEE Transactions on Geoscience and Remote Sensing*, vol. 47, no. 11, 2009.
- [8] M. E. Winter, "N-FINDR: an algorithm for fast autonomous spectral end-member determination in hyperspectral data," *Proc. SPIE Image Spectrometry V*, vol. 3753, pp. 266–277, 2003.
- [9] J. C. Harsanyi and C.-I Chang, "Hyperspectral image classification and dimensionality reduction: orthogonal subspace projection," *IEEE Transactions on Geoscience and Remote Sensing*, vol. 32, no. 4, pp. 779–785, 1994.
- [10] J. M. P. Nascimento and J. M. Bioucas-Dias, "Vertex Component Analysis: A Fast Algorithm to Unmix Hyperspectral Data," *IEEE Transactions on Geoscience and Remote Sensing*, vol. 43, no. 4, pp. 898–910, 2005.
- [11] C.-I Chang, *Hyperspectral Imaging: Techniques for Spectral Detection and Classification*, Kluwer Academic/Plenum Publishers: New York, 2003.